Short Papers

A Transition from Rectangular to Nonradiating Dielectric Waveguide

J. A. G. MALHERBE, SENIOR MEMBER, IEEE,
J. H. CLOETE, MEMBER, IEEE, AND I. E. LÖSCH

Abstract—**A transition between standard *X*-band waveguide and nonradiating dielectric (NRD) waveguide is described. It consists of a transition from air-filled rectangular waveguide to reduced-width dielectric-filled waveguide, cascaded with a transition to NRD. Both transitions are theoretically designed to provide both mode matching as well as a low reflection coefficient. The composite transition can be used for measurements in NRD while making use of conventional waveguide test equipment.**

I. Introduction

A transmission medium with potential application in the millimeter-wave region is the nonradiating dielectric (NRD) waveguide [1]–[6]. In this medium, a dielectric strip is sandwiched between two metal plates. In the frequency band of operation, the air-filled region between the plates is below cutoff for an appropriately polarized wave, while the dielectric-filled region constitutes a guide above cutoff. Thus, the wave is trapped in the vicinity of the dielectric and radiation cannot take place at bends, a common problem with other dielectric waveguides. NRD physically resembles *H*-guide described 30 years ago by Tischer [17]; however, the crucial idea of reducing the plate spacing to less than a half-wavelength to prevent radiation is attributed to Yoneyama and Nishida [18, pp. 1036 and 1042]. The idea was independently conceived by Malherbe during a sabbatical at the University of Illinois [19].

This paper describes the development of a good quality transition between standard *X*-band waveguide and NRD waveguide. Such a transition enables the use of conventional waveguide test equipment for measurements on NRD components or circuits. The development and testing of this transition was done in *X*-band for ease of manufacture and low cost. The design is based on a theoretical procedure rather than on empirical methods as described in [7].

II. Physical Description

The composite transition consists of two sections, as shown in Fig. 1. The first part is a transition between standard rectangular *X*-band waveguide of inside dimensions 22.86×10.16 mm, and a reduced-width, dielectric-filled metal waveguide of dimensions 15.00×10.16 mm. The dielectric used was Polypenco Q200.5 cross-linked polystyrene with $\epsilon_r = 2.55$, which was chosen for its low-loss properties as well as its excellent machinability. The metal sidewalls are linearly tapered for ease of machining, while the dielectric taper approximates a specified impedance match as well as maintaining mode matching. The cross section AA' of this region is shown in Fig. 2(a), where both c and a are variables.

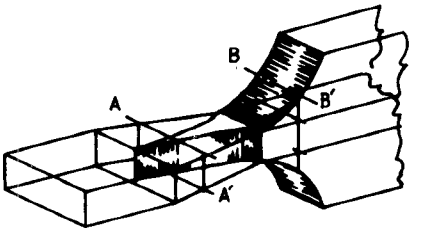

Fig. 1. Composite transition.

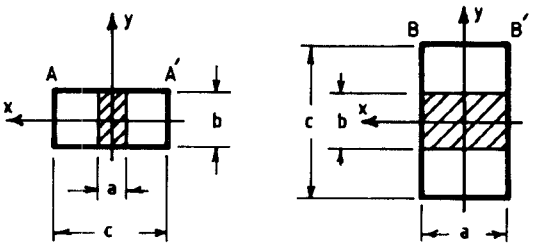

Fig. 2. Two nonhomogeneous cross sections.

The second transition is between the reduced-width guide and NRD, where the width is now kept constant at the plate separation value of $a = 15$ mm. The dielectric height b is kept constant at 10.16 mm, while the metal height c is variable, as shown in cross section BB', in Fig. 2(b). The rate of change of c is once again calculated for a specified impedance match, while the TE_{10}-mode that exists in the uniformly filled region is gradually converted to the dominant NRD mode, a hybrid mode.

III. Propagation in *E*-Plane Slab-Loaded Rectangular Waveguide

It is known [8], [12], [14] that for the class of inhomogeneously filled rectangular waveguides where the boundaries between the different dielectric media are parallel to only one of the axes, the modes can be found relatively simply using potential functions. The structures shown in Fig. 2 are members of this class. The modes are either transverse electric (TE) or longitudinal section electric (LSE) with respect to the dielectric interface, or transverse magnetic (TM) or longitudinal section magnetic (LSM) with respect to the dielectric interface. The modes can be derived from a single vector potential directed normal to the interface. In general, the modes are hybrid but it is also known for the case of Fig. 2(a) that with the electric field parallel to the slab and no variation of the fields along the air–dielectric interface, the modes are also TE to the direction of propagation and are not hybrid. Gardiol [15] refers to these as "distorted" TE_{m0} modes. In fact, for the partially filled guide of Fig. 2(a), the dominant LSE or TE_x mode reduces to the TE_{10} mode of a homogeneously filled rectangular guide for the two special cases $a = 0$ and $a = c$. Consequently, the partially filled guide will serve as a natural transition from air to dielectric-filled waveguide.

Manuscript received September 10, 1984; revised January 15, 1985. This work was supported in part by Barlow Electronic Holdings.

J. A. G. Malherbe and I. E. Lösch are with the Department of Electronic Engineering and Laboratory for Advanced Engineering, University of Pretoria, 0002 South Africa.

J. H. Cloete was with the University of Pretoria. He is now with the Department of Electrical and Electronic Engineering, University of Stellenbosch, 7600 South Africa.

0018-9480/85/0600-0539$01.00 ©1985 IEEE

It is of practical interest to note that while a pyramidal taper may seem to be a good candidate for realizing the transition, a hybrid mode is required to satisfy the boundary conditions [14] making the pyramidal taper less suitable than the one-dimensional taper in the H-plane.

The structure of Fig. 2(a) has been studied in detail [13], [15], and the derivation of the fields using potential theory is straightforward [8], [12]. Using Harrington's formulation, the choice of the magnetic vector potential $\bar{A} \equiv 0$ and the electric vector potential

$$\bar{F} = \bar{a}_x \psi(x, y) \tag{1}$$

with the propagation factor $e^{j(\omega t - \beta_g z)}$ suppressed yields the LSE or TE_x modes with no electric-field component normal to the dielectric surface [8, p. 153].

The appropriate form for the potential function is

$$\psi(x, y) = \cos(\beta_{x1} x) \tag{2}$$

in the dielectric-filled region, and

$$\psi(x, y) = K_1 \sin(\beta_{x2} |c/2 - x|) \tag{3}$$

in the air-filled region. Since the potential function satisfies the scalar wave equation [8, p. 129] in both regions, the eigenvalues are related as follows:

$$\beta_g^2 = \epsilon_r k_0^2 - \beta_{x1}^2 = k_0^2 - \beta_{x2}^2 \tag{4}$$

where $k_0^2 = \omega^2 \mu_0 \epsilon_0$.

By imposing field continuity conditions at the air–dielectric interface, the following expression is obtained:

$$\beta_{x1} \tan(\beta_{x1} a/2) = \beta_{x2} \cot(\beta_{x2}(c - a)/2). \tag{5}$$

The eigenvalues for the dominant mode can be obtained by solving (4) and (5) numerically. The field distributions and the parameters of major interest, the guide wavelength

$$\lambda_g = \lambda_0 \left(1 - (\beta_{x2}/k_0)^2\right)^{-1/2} \tag{6}$$

and the wave impedance

$$Z = 376.7 \lambda_g / \lambda_0 \tag{7}$$

can then be computed where $Z = -E_y/H_x$.

IV. Propagation in H-Plane Slab-Loaded Rectangular Waveguide

The structure shown in Fig. 2(b) serves as a natural transition from homogeneous dielectric-filled rectangular waveguide to NRD when c is increased from $c = b$ to $c \gg b$. This is because the dominant TM_y or LSM mode in the general structure $c > b$ reduces to the TE_{10} mode in the homogeneous structure $c = b$.

The choice of the electric vector potential function $\bar{F} \equiv 0$ and the magnetic vector potential function

$$\bar{A} = \bar{a}_y \psi(x, y) \tag{8}$$

with the propagation factor $e^{j(\omega t - \beta_g z)}$ suppressed as before, yields the LSM or TM_y modes with no magnetic-field components normal to the dielectric surface [8, p. 153].

In this case, the appropriate potential functions are given by

$$\psi(x, y) = \cos(\pi x/a) \cos(\beta_y y) \tag{9}$$

in the dielectric-filled region and

$$\psi(x, y) = K_2 \cos(\pi x/a) \cosh\left([c/2 - y] v_y\right) \tag{10}$$

in the air-filled region. The relationship between the eigenvalues

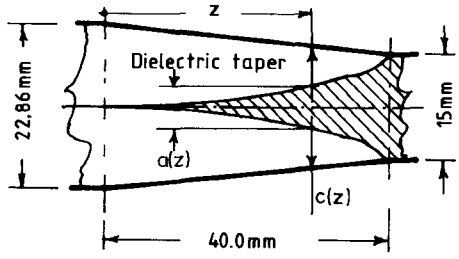

Fig. 3. Transition from standard X-band air-filled to dielectric-filled waveguide, to scale.

is obtained from the scalar wave equation

$$\beta_g^2 = \epsilon_r k_0^2 - \beta_y^2 - \left(\frac{\pi}{a}\right)^2 = k_0^2 + v_y^2 - \left(\frac{\pi}{a}\right)^2. \tag{11}$$

As before, from continuity conditions

$$\tan\left(\beta_y \frac{b}{2}\right) \coth\left[(c/2 - b/2) v_y\right] = \frac{\epsilon_r v_y}{\beta_y}. \tag{12}$$

The eigenvalues for the fundamental mode can be obtained by solving (11) and (12) numerically. The field distributions and the guide wavelength

$$\lambda_g = \lambda_0 \left(1 + (v_y/k_0)^2 - (\lambda_0/2a)^2\right)^{-1/2} \tag{13}$$

and wave impedance in the dielectric region

$$Z = \left(\beta_g^2 + (\pi/a)^2\right) / (\omega \epsilon_0 \epsilon_r \beta_g) \tag{14}$$

can then be computed where $Z = -E_y/H_x$.

V. Transition from Air- to Dielectric-Filled Waveguide

Klopfenstein [9] and Hecken [10] describe tapers for matching transmission lines of different impedances. The Klopfenstein design is optimal in that, for a given Dolph–Tchebyshev equal-ripple response, it yields the shortest possible taper. It has, however, the disadvantage of a discontinuity in the geometry at each end of the taper. The Hecken taper was chosen because for the same passband reflection coefficient it is only slightly longer than the Klopfenstein design, but without the discontinuities.

The geometry of the transition is shown in Fig. 3. For ease of manufacture, the metal walls were tapered linearly from c_1 to c_2 over the length l, so that

$$c(z) = c_1 + (c_2 - c_1) z/l. \tag{15}$$

It therefore remains to determine the width $a(z)$, $0 \leq z \leq l$. The appropriate impedance to use for the taper design is the wave impedance [10], [11, p. 257], and the assumption is made that only the dominant mode propagates.

The guide wavelength at the homogeneous extremities are given directly by

$$\lambda_g/\lambda_0 = \left[1 - (\lambda_0/2c_1)^2\right]^{-1/2} \tag{16}$$

for $z = 0$, and by

$$\lambda_g/\lambda_0 = \left[\epsilon_r - (\lambda_0/2c_2)^2\right]^{-1/2} \tag{17}$$

for $z = l$, where λ_0 is the free-space wavelength. The wave impedance is given by (7).

The parameters at the extremities are shown in Table I for $\epsilon_r = 2.55$, $c_1 = 22.86$ mm, and $c_2 = 15.00$ at $f = 9$ GHz.

The inherent return loss (for $l = 0$) is -12 dB, and a taper with -25-dB ripple will therefore result in a theoretical return loss of -37 dB. From [10, table I], the values of $B = 3.2136$ and $\beta l_{\min} = 4.1046$ are obtained. The values of $G(B, \xi)$ versus ξ are

TABLE I
WAVEGUIDE PARAMETERS AT EXTREMITIES OF TAPER

Position	$z=0$	$z=l$
Wave impedance Z	550.4 Ω	328.4 Ω
Guide wavelength λ_g	48.70 mm	29.06 mm
Cutoff frequency f_c	6.56 GHz	6.26 GHz

TABLE II
PARAMETERS FOR TRANSITION FROM AIR-FILLED TO DIELECTRIC-FILLED WAVEGUIDE

ξ	$G(B,\xi)$	$Z(\xi)$ (Ω)	z (mm)	$a(z)$ (mm)	$c(z)$ (mm)
−1.0	−1.00000	550.4	0.0	0.00	22.86
−0.8	−0.91901	539.0	5.1	0.50	21.80
−0.6	−0.77302	519.1	10.0	1.05	20.90
−0.4	−0.56117	491.4	14.7	1.70	19.97
−0.2	−0.29565	458.9	19.0	2.50	19.13
0.0	0	425.1	23.1	3.40	18.32
0.2	0.29565	393.9	26.8	4.50	17.59
0.4	0.56117	367.8	30.3	5.80	16.91
0.6	0.77301	348.2	33.7	7.30	16.24
0.8	0.91901	335.3	36.9	9.10	15.61
1.0	1.00000	328.4	40.0	15.00	15.00

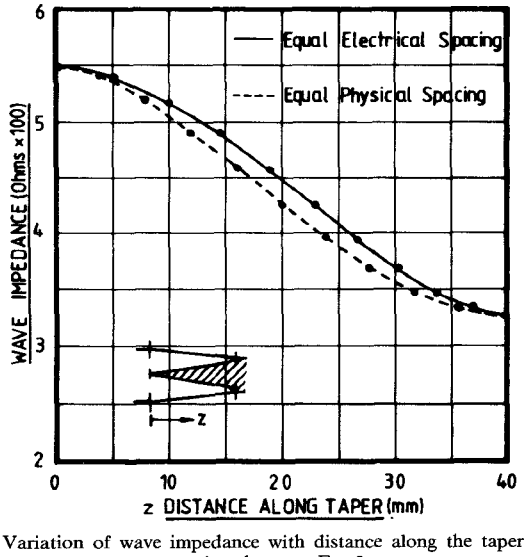

Fig. 4. Variation of wave impedance with distance along the taper for the transition shown in Fig. 3.

also obtained and are shown in Table II. $G(B,\xi)$ is a transcendental function that quantifies the impedance taper as a function of normalized distance $\xi = 2z/l - 1$.

The normalized distance ξ corresponds to equal spacings in a TEM-line. However, in this case, the propagation velocity and wave impedance both vary strongly as the dimensions change. Consequently, the impedance values $Z(\xi)$ must be made to correspond to points of equal *electrical* spacing.

The design procedure for a chosen taper length of 40 mm is as follows. First, the points ξ are equally spaced, and the dimensions $a(\xi)$ and $c(\xi)$ calculated to give the desired values of $Z(\xi)$, using (4)–(7). This is a first estimate. Corresponding values of λ_g are now calculated, the physical spacing adjusted for equal electrical spacing, and the process repeated. This iterative approach continues until the values of $Z(\xi)$ and λ_g converge. The variation of $Z(z)$ versus z is shown in Fig. 4, for both the cases of equal electrical and physical spacing. The final set of spacings and dimensions for the taper is shown in Table II, while the taper is shown to scale in Fig. 3.

TABLE III
PARAMETERS FOR TRANSITION FROM DIELECTRIC-FILLED WAVEGUIDE TO NRD

ξ	$G(B,\xi)$	$Z(\xi)$ (Ω)	z' (mm)	$c(z')$ mm
−1.0	−1.00000	335.6	0.0	10.16
−0.8	−0.94298	341.0	2.5	11.48
−0.6	−0.81521	353.3	5.4	13.26
−0.4	−0.60578	374.5	8.8	14.3
−0.2	−0.32412	405.1	12.8	17.02
0.0	0	443.3	17.3	22.80
0.2	0.32412	485.2	22.7	27.80
0.4	0.60578	524.7	28.7	33.82
0.6	0.81521	556.2	35.2	41.34
0.8	0.94298	576.4	42.1	51.80
1.0	1.00000	585.6	49.27	81.28

VI. TRANSITION FROM DIELECTRIC-FILLED WAVEGUIDE TO NRD

The transition from dielectric-filled waveguide to NRD is simplified somewhat by the fact that the dielectric dimensions are constant at 10.16×15.0 mm. This means that the taper can be computed more easily, and directly, because only the plate separation c is a variable. For the design of the second taper, it was decided to choose a cutoff frequency of 8.8 GHz to ensure satisfactory performance from 9 GHz upwards. The start and stop values of the wave impedance were, respectively, 335.6 Ω and 585.6 Ω, giving a return loss of −11.3 dB for a zero-length transition. In order to have an overall theoretical reflection coefficient which is better than −30 dB for the composite transition, this second transition was designed to a total reflection coefficient ripple level of better than −40 dB, necessitating a taper design of −30-dB reflection level.

For this case, from [10, table I], for $B = 4.0091$, it follows that $\beta l_{\min} = 4.7533$. The total electrical length of the taper was divided into 20 equal sections. For each section, the desired impedance was calculated, and then the dimensions that realize that impedance. Having the dimensions, the guide wavelength at each of these points was calculated, and the average between two successive steps used to calculate the physical separation for equal electrical lengths.

Table III shows the design values of $\xi, G(B,\xi)$, and Z as well as the calculated values for plate separation $c(z')$ versus distance from the start of the transition z'.

The physical dimensions of the taper are shown in Fig. 5, while the variation of impedance with distance along the taper is shown in Fig. 6 for both equal electrical and physical spacing. In this case, the differences are even greater than before.

Fig. 7 shows a photograph of the taper with the dielectric in position in the NRD, and the metal taper on the transition to dielectric-filled waveguide removed.

VII. MEASUREMENT

A back-to-back pair of the first type of transition was manufactured with 250 mm of reduced-width guide separating the two transitions. The output transition was terminated in a matched load and the input reflection coefficient, as measured with a waveguide reflectometer, is shown in Fig. 8. Due to reflections

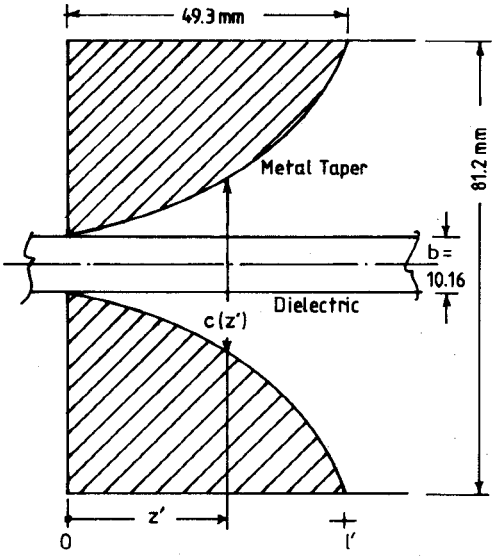

Fig. 5. Transition from dielectric-filled waveguide to NRD, to scale.

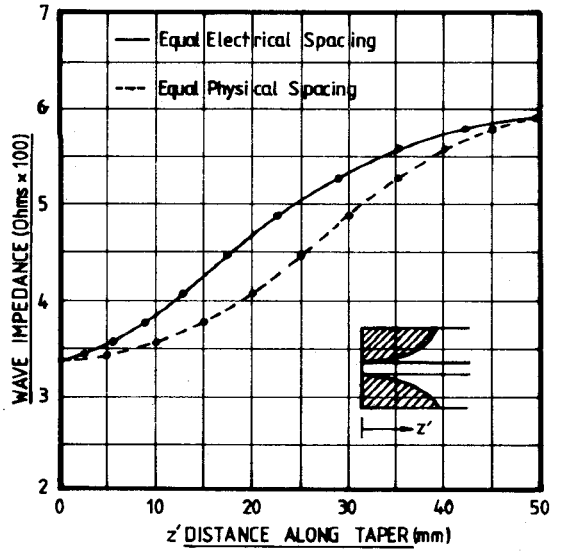

Fig. 6. Variation of wave impedance with distance along the taper for the transition shown in Fig. 5.

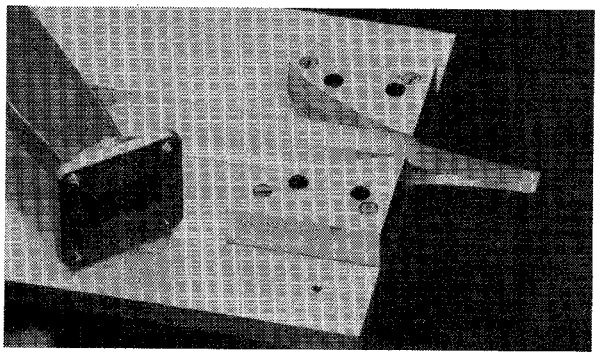

Fig. 7. Photograph of transition with the metal taper and one NRD side removed.

from both ends, separated by a length of line, constructive and destructive interference results, giving rise to the oscillating response of Fig. 8. Assuming equal reflections at each end, the broken line in Fig. 8 was calculated as the performance of a single transition. The measured reflection coefficient is approxi-

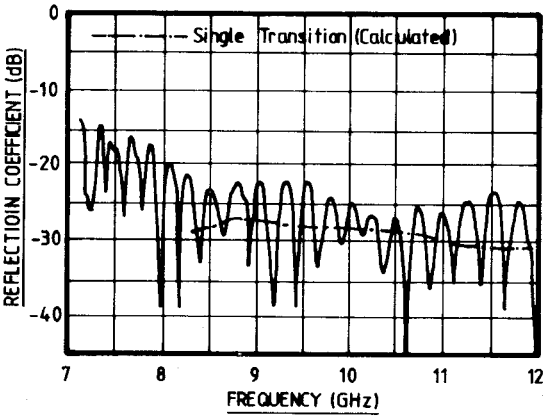

Fig. 8. Measured performance of two back-to-back transitions between air- and dielectric-filled waveguide, separated by 250 mm of dielctric-filled guide.

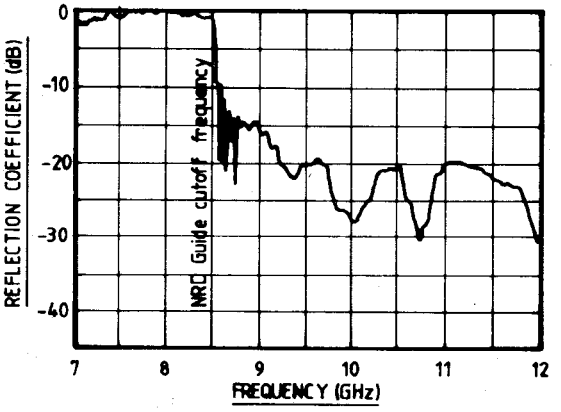

Fig. 9. Measured performance of the composite transition between standard waveguide and terminated NRD.

mately 10 dB greater than the theoretical reflection coefficient of a perfect transition. This is ascribed primarily to inaccuracies in the manufacture of the dielectric taper and junction effects.

Two sets of complete transitions, separated by 800 mm of NRD were also manufactured, but the interference problem was too complex for analysis. Consequently, an NRD termination was made by laying two strips of Eccoshield FGM 40, each 200 mm long and 15 mm wide, on either side of the dielectric, with the leading ends pulled away to the same shape as the launching taper. The reflection coefficient versus frequency response is shown in Fig. 9 and is less than -25 dB over 25 percent of the 9–12-GHz band, and less than -20 dB over 85 percent of the band. The performance was satisfactory for an experimental program on a slotted NRD waveguide array [16].

VIII. Conclusion

An analytical design procedure for a composite transition between conventional and NRD waveguide has been described. The design goal for the experimental transition was a reflection coefficient of less than -30 dB over the band from 9–12 GHz. The disappointing experimental results are presently ascribed primarily to inaccurate machining of the dielectric taper, but also to junction effects and unknown performance of the NRD termination. These results should not detract from the systematic and quantitative design procedure. The effect of deviations from the theoretical dimensions, due to manufacturing errors, on the electrical performance requires study in order to be able to specify tolerances.

For applications at millimeter wavelengths, the usefulness of this transition will depend on the ability to fabricate the dielectric

taper. Conventional machining of the taper may be impractical, but other techniques can be devised. It is, however, emphasized that the transition described here was not intended for production but for a specific measurement program [16].

ACKNOWLEDGMENT

The authors wish to express their appreciation to W. Wibbelink and J. Brand for the manufacture of the trial transition.

REFERENCES

[1] T. Yoneyama and S. Nishida, "Nonradiative dielectric waveguide for millimeter-wave integrated circuits," *IEEE Trans. Microwave Theory Tech.*, vol. MTT-29, pp. 1188–1192, Nov. 1981.

[2] T. Yoneyama, S. Nishida, and M. Yamaguchi, "Bends in nonradiative dielectric waveguide," in *1982 IEEE MTT-S Dig.*, pp. 300–301.

[3] T. Yoneyama, M. Yamaguchi, and S. Nishida, "Bends in nonradiative dielectric waveguide," *IEEE Trans. Microwave Theory Tech.*, vol. MTT-30, pp. 2146–2150, Dec. 1982.

[4] T. Yoneyama, N. Tozawa, and S. Nishida, "Coupling characteristics of nonradiative dielectric waveguides," *IEEE Trans. Microwave Theory Tech.*, vol. MTT-31, pp. 648–654, Aug. 1983.

[5] T. Yoneyama and S. Nishida, "Nonradiative dielectric waveguide circuit components," *Int. J. Infrared and Millimeter Waves*, vol. 4, no. 3, 1983.

[6] T. Yoneyama, S. Fujita, and S. Nishida, "Insulated nonradiative dielectric waveguide for millimeter-wave integrated circuits," *IEEE Trans. Microwave Theory Tech.*, vol. MTT-31, pp. 1002–1008, Dec. 1983.

[7] J. A. G. Malherbe, T. N. Trinh, and R. Mittra, "Transition from metal to dielectric waveguide," *Microwave J.*, vol. 23, no. 11, pp. 71–74, Nov. 1980.

[8] R. F. Harrington, *Time-Harmonic Electromagnetic Fields*. New York: McGraw-Hill, 1961.

[9] R. W. Klopfenstein, "A transmission line taper of improved design," *Proc. IRE*, vol. 44, pp. 31–35, Jan 1956.

[10] R. P. Hecken, "A near-optimum matching section without discontinuities," *IEEE Trans. Microwave Theory Tech.*, vol. MTT-20, pp. 734–739, Nov. 1972.

[11] R. E. Collin, *Foundations for Microwave Engineering*. New York: McGraw-Hill, 1966.

[12] R. E. Collin, *Field Theory of Guided Waves*. New York: McGraw-Hill, 1960.

[13] P. H. Vartanian, W. P. Ayres, and A. I. Helgesson, "Propagation in dielectric slab loaded rectangular guide," *IRE Trans. Microwave Theory Tech.*, vol. MTT-6, pp. 215–222, Apr. 1958.

[14] W. Schlosser and H-G. Unger, "Partially filled waveguides and surface waveguides of rectangular cross section," in *Advances in Microwaves*, vol. 1, L. Young, Ed. New York: Academic Press, 1966, pp. 319–387.

[15] F. E. Gardiol, "Higher-order modes in dielectrically loaded rectangular waveguides," *IEEE Trans. Microwave Theory Tech.*, vol. MTT-16, pp. 919–924, Nov. 1968.

[16] J. A. G. Malherbe *et al.*, "The design of a slot array in nonradiating dielectric waveguide—Part II: Experiment," *IEEE Trans. Antennas Propagat.*, vol. AP-32, pp. 1341–1344, Dec. 1984.

[17] F. A. Benson and F. J. Tischer, "Some guiding structures for millimeter waves," *Proc. Inst. Elec. Eng.*, vol. 131, pt. A, no. 7, pp. 429–449, Sept. 1984.

[18] A. A. Oliner, "Historical perspectives on microwave field theory," *IEEE Trans. Microwave Theory Tech.*, vol. MTT-32, pp. 1022–1045, Sept. 1984.

[19] J. A. G. Malherbe, laboratory notebook, Univ. of Illinois, May 8, 1979.

A Low-Noise GaAs Monolithic Broad-Band Amplifier Using a Drain Current Saving Technique

K. OSAFUNE, N. KATO, T. SUGETA, AND Y. YAMAO

Abstract—**A low-noise and low-power GaAs monolithic broad-band amplifier is proposed and has been developed, which has a new cascade connection with a large gate-width input FET and the other circuits in such a way that the output stage current flows through the input FET. The fabricated amplifier operates on +5-V single supply voltage, and provides a 3.3-dB noise figure, less than 180-mW power dissipation, and a 10-MHz–2.0-GHz bandwidth with 16-dB gain.**

Manuscript received August 25, 1984; revised January 15, 1985.

K. Osafune, N. Kato, and T. Sugeta are with Atsugi Electrical Communication Laboratory, Nippon Telegraph and Telephone Public Corporation, Atsugi, Japan.

Y. Yamao is with Yokosuka Electrical Communication Laboratory, Nippon Telegraph and Telephone Public Corporation, Yokosuka, Japan.

I. INTRODUCTION

Recent advances in GaAs IC technology make it possible to develop GaAs monolithic broad-band amplifiers for mobile radio applications. For these amplifiers, both a low dc power dissipation and a low noise figure are required. From a practical point of view, single-power supply operation and good input/output matching are desirable. To meet these needs, low-noise, low power-dissipation GaAs monolithic broad-band amplifiers were developed [1]–[3]. They achieved a low noise figure and good input/output matching by using RC parallel feedback, and also achieved low power dissipation by using inductive loads (choke coils). Although inductive loads are effective in reducing amplifier power dissipation, choke coil sizes are almost 10 times as large as IC chips below the S-band.

In this short paper, we propose a new circuit construction which enables both power saving and low-noise operation in the monolithic GaAs amplifier for VHF–UHF mobile radio systems. Design considerations and performance characteristics of this amplifier are described as follows.

II. CIRCUIT DESIGN

In order to construct a low-noise amplifier, it is desirable to increase the input-stage FET transconductance g_m. Therefore, the input-stage FET must have a wide gate width to afford high g_m. To make input matching, a resistor negative feedback circuit is advantageous from the view point of low-noise characteristics. Furthermore, if the amplifier open-loop gain is high, the feedback resistor can be increased, and the noise generated from the feedback resistor can be suppressed. For increasing the open-loop gain, multistage construction is effective [2]. But dc drain current also increases as the number of the stages increases. If we can get high gain without a drain current increase, both a low noise figure and low power dissipation are possible.

For this purpose, a new circuit construction amplifier (shown in Fig. 1) has been developed. This amplifier consists of three stages; the input stage ($Q1, Q2$) and two source follower stages ($Q3, Q4$ and $Q5, Q6$). The input stage owns a wide-gate input FET $Q1$ and a relatively high-impedance resistor load R_d to obtain both a low noise figure and high gain. The amplifier open-loop gain is mainly determined by this stage. The two source follower stages do not amplify signal voltages, but they do lower the amplifier output impedance to 50 Ω. The small input capacitance of the intermediate source follower FET $Q3$ makes it possible to increase the resistor load R_d without decreasing the amplifier bandwidth; thus, the open-loop gain increases as well. The output matching is performed by determining the transconductance of the output FET $Q5$ equal to 20 mS ($=1/50$ Ω). A negative feedback circuit (R_f, C_f) is used for input matching with little influence on the noise figure. The gate-grounded FET $Q2$ is used to make the input FET drain voltage constant and yields bias voltages of current source FET's $Q4$ and $Q6$.

In this construction, the bias currents of two source follower stages pass through $Q1$. Therefore, the amplifier's total drain current is equal to that of the input FET $Q1$. Due to the adoption of this multistage cascade construction, high gain and a low noise figure are attained without an increase in current.

0018-9480/85/0600-0543$01.00 ©1985 IEEE